

# Dilepton production in $p + p$ , $Cu + Cu$ and $Au + Au$ collisions at $\sqrt{s} = 200$ GeV

J. Manninen<sup>1</sup>, E. L. Bratkovskaya<sup>2</sup>, W. Cassing<sup>1</sup>, O. Linnyk<sup>2</sup>

<sup>1</sup> Institut für Theoretische Physik, Universität Giessen, 35392 Giessen, Germany

<sup>2</sup> Institut für Theoretische Physik, Universität Frankfurt, 60054 Frankfurt, Germany

the date of receipt and acceptance should be inserted later

**Abstract.** We study dilepton production in proton-proton,  $Cu + Cu$  as well as in  $Au + Au$  collisions at the center-of-mass energy  $\sqrt{s}=200$  GeV per participating nucleon pair within an extended statistical hadronization model. In extension to earlier studies we incorporate transport calculations for an estimate of uncorrelated  $e^+e^-$ -pairs from semileptonic  $D$  meson decays. While the invariant mass spectrum of dielectrons is well understood in the  $p + p$  collisions, severe discrepancies among different model scenarios based on hadronic degrees of freedom and recent data from the PHENIX Collaboration are found in heavy-ion collisions in the low mass region from 0.15 to 0.6 GeV as well as in the intermediate mass regime from 1.1 to 3 GeV when employing the standard dilepton sources. We investigate, furthermore, the background from correlated dileptons that are not emitted as a pair from a parent hadron but emerge from semileptonic decays of two correlated daughter hadrons. Our calculations suggest a sizeable contribution of such sources in central heavy-ion collisions in the low mass region. However, even the upper limits of our calculations are found to be far below the dilepton mass spectra of the PHENIX Collaboration.

**PACS.** 25.75.-q – 13.60.Le – 14.40.Lb – 14.65.Dw

Revised version: 18th March 2011

## 1 Introduction

The goal of this work is to study the production of correlated electron-positron pairs in proton-proton and heavy-ion collisions at  $\sqrt{s_{NN}}=200$  GeV. We will evaluate the invariant mass spectrum  $dN/dm_{e^+e^-}$  within an extended hadronization model up to invariant masses of 4 GeV thus covering the low mass as well as the intermediate mass and charmonium regime. We confront our calculations with corresponding measurements of the PHENIX collaboration (within the experimental acceptance) which has taken data [1, 2] up to 4 GeV in  $m_{e^+e^-}$  at mid-rapidity. In the case of proton-proton collisions the PHENIX collaboration has found out that the measured spectrum can be described very well up to masses of 4 GeV, if one takes into account all relevant hadronic sources of dileptons in the analysis. This was done by a simultaneous measurement of all hadron rapidity densities and transverse momentum spectra around mid-rapidity; by using these experimental rapidity densities one can then estimate the dilepton yields at different invariant masses due to the known hadronic decays to  $e^+e^-$  pairs. Independently, microscopic transport calculations within the Hadron-String-Dynamics (HSD) framework [3, 4] have come to the same

conclusion when incorporating the measured cross section for  $c\bar{c}$  pairs from the PHENIX collaboration [5].

In contrast to the proton-proton collisions, the measured invariant mass spectrum of dileptons in  $Au + Au$  collisions have so far not been properly understood theoretically. Instead, theoretical estimates are found to deviate up to a factor of 4 or 5 from the PHENIX data for central Au+Au collisions in the low mass regime [5, ?] (cf. also Fig. 42 in Ref. [2]) and by up to a factor 2 to 3 for intermediate masses. Such discrepancies among (hadronic) models and experimental data have not been observed at lower Super-Proton-Synchrotron (SPS) beam energies and in different collision systems [5, 7] where a major broadening of the vector-meson resonances is reported. This might suggest that non-hadronic dilepton channels could be responsible for the discrepancies observed so far. This issue needs further independent investigations.

In this work, we will partly repeat the analysis by the PHENIX collaboration in the intermediate mass range especially with respect to the contribution from charmed meson decays but instead of using the measured yields as input for the dilepton sources, we wish to implement different models in order to calculate the rapidity densities of different hadrons and subsequently estimate the emission of dileptons from their decays. These models are controlled by the PHENIX data for  $p + p$  collisions.

We recall that the invariant mass spectrum of dileptons can be divided in three fairly distinct regions in each of which different physics processes are dominant. Below the  $\phi$  meson mass, the region referred hereafter as the low mass region (LMR:  $m_{e^+e^-} \in [0.0 ; 1.1]$  GeV), the dilepton production is dominated by the decays of non-charmed mesons, i.e. mesons with essentially light quark content ( $u, d, s$ ). In the intermediate mass region (IMR:  $m_{e^+e^-} \in [1.1 ; 3.2]$  GeV), i.e. in between the  $\phi$  meson and  $J/\psi$  mass, the invariant mass spectrum of electron-positron pairs is dominated by the semileptonic decay products of open charm mesons. Strictly speaking this is just a background for the "true" dilepton sources, but since this component is always present in the analysis, one needs to carefully evaluate the contribution from open charm as well. Furthermore, above about 3 GeV of invariant mass the direct decays of charmonia become dominant and provide a constraint on the number of produced  $c\bar{c}$ -pairs - forming bound states - once the charmonium suppression is controlled independently. We concentrate in this article on studying the LMR and IMR thus exceeding previous approaches that focused on the LMR and extrapolated to the IMR. The high mass region (HMR:  $m_{e^+e^-} > 3.8$  GeV) of the dilepton invariant mass spectrum is dominated by the Drell-Yan process and  $B$  meson decays which we will not address here.

In describing the yields or ratios of particle yields of hadrons consisting of  $u, d$  and  $s$  quarks phenomenological models, in particular "thermal models", have proven to be very useful due to their simplicity and low number of adjustable parameters. In this work, we will evaluate the yields of light mesons within the statistical hadronization model which has been applied to high-energy elementary [8–10] and especially heavy-ion [11–21] collision experiments in order to calculate the yields of different hadron species with fairly a lot of success. We mention that the CERES Collaboration has also analyzed their dilepton data in the LMR on the basis of the statistical hadronization model with some success at Super-Proton-Synchrotron (SPS) energies for  $Pb + Au$  collisions [22].

Unlike for the bulk meson production in the LMR, the statistical hadronization model can not be applied to estimate the yields of charmed hadrons in the IMR. Instead, we need to rely on experimental information here in order to estimate the differential yields of charmed hadrons. To this aim we will formulate an 'extended statistical model' including early charm-pair production, collective flow of the hot and dense matter as well as correlated and uncorrelated semileptonic decays of  $D$  mesons. The amount of  $D$  meson rescattering will be followed up by the HSD transport approach [23] in order to estimate the amount of surviving correlated semileptonic decays in the heavy-ion collisions.

In extension to earlier studies we will, furthermore, explore the contribution of correlated semileptonic decays stemming from kaon-antikaon pairs that emerge from the decay of heavy parent hadrons. The most important of these sources are proportional to  $\gamma_S^2$ , where  $\gamma_S$  denotes the strangeness suppression factor which is low in proton-

proton reactions but close to unity in nucleus-nucleus collisions. Our upper limits for these contribution will be compared to the PHENIX data within the proper acceptance windows as well as the conventional dilepton sources mentioned above.

## 2 An extended statistical hadronization model

The statistical hadronization model (SHM) has been applied successfully in calculating the number of emitted hadrons in high-energy collision systems [8–21]. This model is well documented in the references given above and accordingly we will introduce the main concepts only. We evaluate the hadron yields in the grand-canonical ensemble because the calculations simplify substantially if one does not require exact conservation of Abelian charges and/or energy-momentum. Our choice is motivated by two reasons: First of all experimental observations show that the grand-canonical ensemble is sufficient enough, i.e. that at RHIC energies the data are well described under the approximations we have chosen. The other reason is that in order to evaluate the hadron yields in the canonical ensembles, one needs to know the volume as well as the exact (integer) charges on an event by event basis. However, the PHENIX collaboration has measured only a small fraction of the emitted hadrons while a large part of the system is never observed. We would need to make severe assumptions for the part of the system not measured, if we were to implement the canonical formalism for the calculation. We also note that the canonical effects are most pronounced for heavy and exotic hadrons, while the bulk of the dilepton emission arises from the low-mass mesons, which are produced abundantly and do not suffer from canonical suppression effects. Thus, we deem that performing the analysis in the grand-canonical ensemble should be good enough for our purposes and indeed this seems to be confirmed by our work (see below).

In the SHM, the primary hadron multiplicity of hadron type  $i$  is calculated (in the on-shell Boltzmann approximation) according to

$$N_i = V \frac{2J_i + 1}{(2\pi)^3} \int \gamma_S^{n_s} e^{\mu \cdot \mathbf{q}_i / T} e^{-\sqrt{p^2 + m_i^2} / T} d^3p. \quad (1)$$

In Eq. (1)  $J_i$  denotes the spin,  $p$  the momentum and  $m_i$  the mass of the particle while  $q_i$  is a vector consisting of the baryon, electric and strangeness charges of the hadron species  $i$ . The state of the "thermal" fireball is specified by its temperature  $T$ , volume  $V$  and chemical potentials (collected in the vector  $\mu$ ) for baryon, electric and strangeness charges.

Several independent experimental measurements have verified that the mid-rapidity region is actually almost net charge free in proton-proton and  $Au + Au$  collisions at  $\sqrt{s_{NN}} = 200$  GeV [24–26]. The baryon chemical potential is expected to be of the order of 30 MeV [19] in central  $Au + Au$  collisions and we have used this value throughout at all centralities while the  $\mu_S$  and  $\mu_Q$  are set to zero.

Once the chemical potentials are fixed, there are three free parameters characterizing our system: the temperature, the strangeness under-saturation parameter  $\gamma_S$  and the overall normalization volume  $V$ . The auxiliary parameter  $\gamma_S$  is necessary to include in our analysis in order to take into account the empirical fact that the strange particle yields are strongly suppressed with respect to SHM estimates in elementary particle collisions. We have chosen  $\gamma_S=0.6$  in our analysis in accordance with statistical hadronization model fits [25,27] to proton-proton collisions at this beam energy. In  $Au + Au$  collisions, the  $\gamma_S$  parameter increases monotonically from the  $p + p$  value to unity as a function of centrality [19] and the effect will be discussed in detail in the forthcoming sections. The common normalization factor  $V$  for all hadron species is determined in different collision systems from the measurements (see below) while for the temperature we have chosen the value  $T = 170$  MeV in all systems based on the SHM fits to proton-proton and  $Au + Au$  data at this beam energy.

We have included the same collection of hadron species in our analysis as has been included in the works quoted above from which we have taken the thermal parameters. The mean primary hadron and resonance yields of each of the hadron species included in the analysis are calculated according to Eq. (1). For resonances with width larger than 2 MeV, Eq. (1) is convoluted with the relativistic Breit-Wigner distribution and integration over the mass and momentum is enforced. Once the mean primary yields are known, we assume that, from event-to-event, the multiplicity distribution of each species is governed by the Poisson distribution characterized by the mean multiplicities evaluated with Eq. (1). We then sample the Poisson distributions for each of the hadron species in each event to obtain the primary multiplicities and choose momenta for every hadron according to the Boltzmann distribution. All unstable resonances are then allowed to decay according to the most recent branching fractions taken from the particle data group tables [28]. This way we know the momenta of every final state particle and thus it is straightforward to take into account any geometrical and kinematical experimental cuts.

We note here that the statistical hadronization model is useful only for evaluating the relative yields of different hadron species since the rapidity and transverse momentum spectra of all hadrons emitted in the high energy collision experiments do not resemble thermal distributions. This is not a problem for us as long as our results do not depend explicitly on the details of the spectra. Indeed, this is the case for the "true" dilepton emission from a single decaying hadron, i.e. the invariant mass of the lepton pair does not depend on the momentum of the parent hadron and neither does the (Lorentz invariant) number of hadrons. Thus, we may evaluate the number of produced hadrons and dileptons within the statistical hadronization model even though the spectra are not correct.

Unfortunately, the discussion above holds true only if the measurement is performed in  $4\pi$ , i.e. if all hadrons are measured or at least if the experiment extrapolates the measured kinematical region to the unmeasured re-

gions as well. The PHENIX dilepton measurement is carried out in a narrow rapidity window around  $y = 0$  and only leptons with  $p_T > 200$  MeV are taken into account. We have also taken into account the azimuthal geometry and effects of the magnetic field on the charged leptons of the PHENIX detector [2], namely, that electrons and positrons (of charge  $q$ ) are accepted in case both of the conditions

$$\phi_{\min} \leq \phi + q \frac{k_{\text{DC}}}{p_T} \leq \phi_{\max} ; k_{\text{DC}} = 0.206 \text{ rad GeV}/c$$

$$\phi_{\min} \leq \phi + q \frac{k_{\text{RICH}}}{p_T} \leq \phi_{\max} ; k_{\text{RICH}} = 0.206 \text{ rad GeV}/c$$

are simultaneously fulfilled. The PHENIX detector consists of two arms with the angular coverage  $\phi_{\min} = -\frac{3}{16}\pi$ ,  $\phi_{\max} = \frac{5}{16}\pi$  and  $\phi_{\min} = \frac{11}{16}\pi$ ,  $\phi_{\max} = \frac{19}{16}\pi$ .

The limited acceptance in rapidity is not a severe problem here due to the approximate boost invariance of the systems around mid-rapidity at top RHIC energies. In order to make the rapidity distributions of non-charmed hadrons wider, we have randomly boosted<sup>1</sup> (event by event) our "fireball" along the beam axis so that the rapidity distributions of pions become compatible with the BRAHMS measurements [29].

On the other hand, the limited acceptance in  $p_T$  raises some problems, because the statistical hadronization model tends to over-populate the low  $p_T$  part of the spectrum compared with the experimental distributions and thus too few leptons hit the PHENIX acceptance window of  $p_T > 200$  MeV. We have solved this problem by assuming that the created clusters' transverse momentum is normally distributed (with mean  $\mu_{p_T}=0$  but  $\langle p_T \rangle > 0$ ) and fitted the width of the clusters'  $p_T$  distribution together with the system volume  $V$  to the PHENIX data [30,31] in  $p + p$  collisions and in 11 different centrality classes in the case of  $Au + Au$  collisions. Comparison of the data and model calculations are shown in Figure 1 for the  $p + p$  (top panel) and central  $Au + Au$  collisions (bottom panel). The description of the data is similar at all centralities. The resulting widths for the clusters' transverse momentum distributions are shown in Figure 2 while the scaling volumes (divided by the volume in proton-proton collisions) are shown in Figure 3.

The dilepton yields are measured in wider centrality classes than the  $p_T$  spectra from which we have determined the  $\sigma_{p_T}$  and  $V$  and thus in the following calculations for dielectrons we have used interpolated values for  $\sigma_{p_T}$  and  $V$  based on the values shown in Figures 2 and 3.

### 3 Decay widths

In the low invariant mass region the dominant sources of (correlated) dileptons are the direct and Dalitz decays of light mesons. The dielectron decay channels taken into account in this analysis are listed in the Table 1. Each of

<sup>1</sup> assuming a Gaussian distribution with width  $\sigma_y = 4.2$

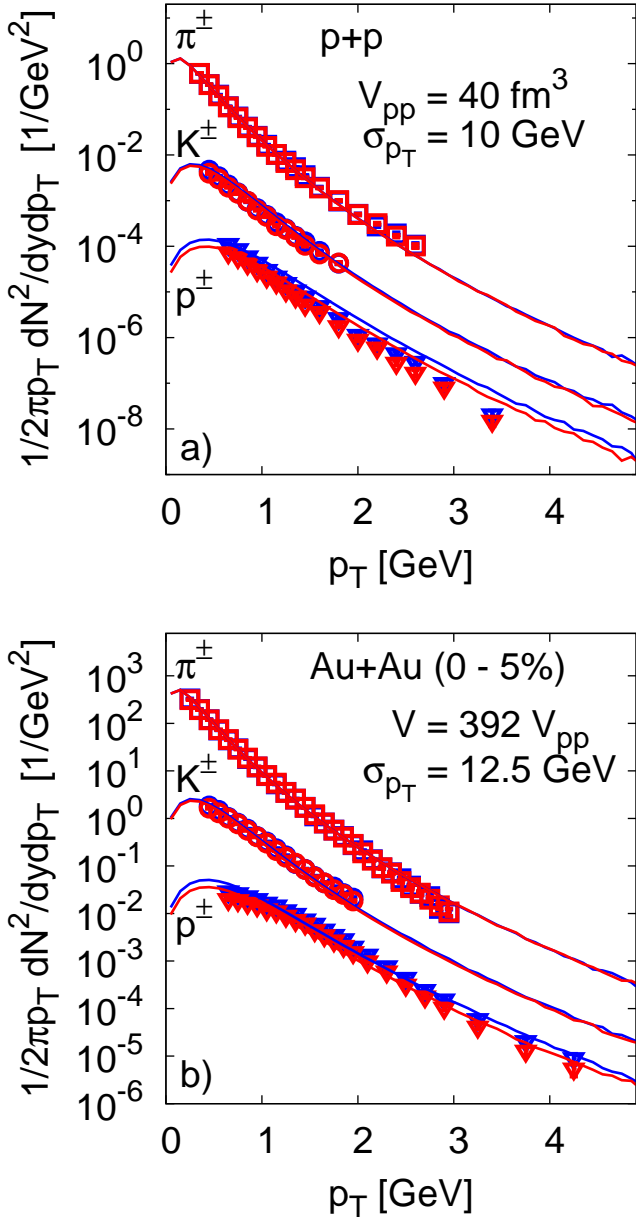


**Fig. 1.** (Color on-line) Transverse momentum spectrum of  $\pi^+$ ,  $\pi^-$ ,  $K^+$ ,  $K^-$ ,  $p$  and  $\bar{p}$  [30,31] in proton-proton collisions (top panel) and (0-5%) most central  $Au + Au$  collisions (bottom panel) at  $\sqrt{s_{NN}}=200$  GeV compared with our model calculations. The width of the clusters' transverse flow profile along with the system volume are fitted to the data shown in the figure. Kaons have been divided by a factor of 10 and nucleons by a factor of 100 for clarity.

the direct decays results in a sharp peak in the mass spectrum at the meson nominal mass while the Dalitz decays yield a continuum spectrum from zero invariant mass up to the mass of the decaying meson. Let us note here that there are many other hadrons and their resonances decaying radiatively into dileptons than the ones listed in Table 1. These could be (and are) important in different kinds of collision systems. For example in heavy-ion collisions

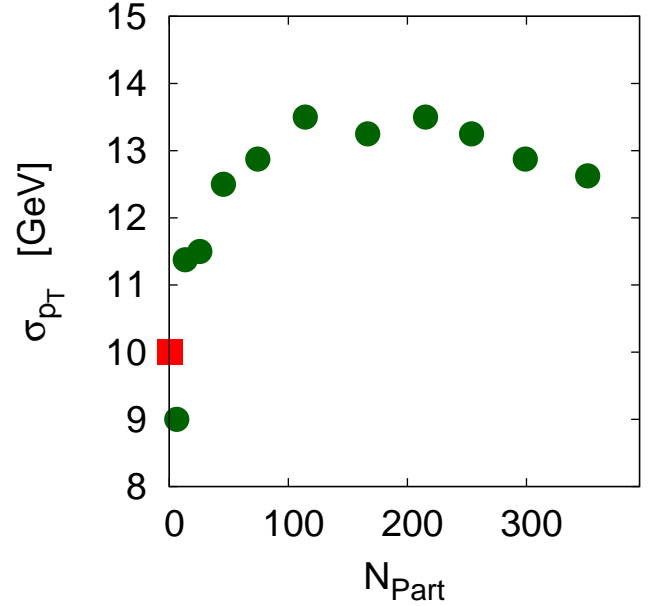


**Fig. 2.** (Color on-line) The width of the clusters' transverse momentum distribution in 11 centrality classes in  $Au + Au$  collisions at  $\sqrt{s_{NN}}=200$  GeV (filled spherical symbols) as a function of the number of participants. The square symbol denotes the width in  $p + p$  collisions.

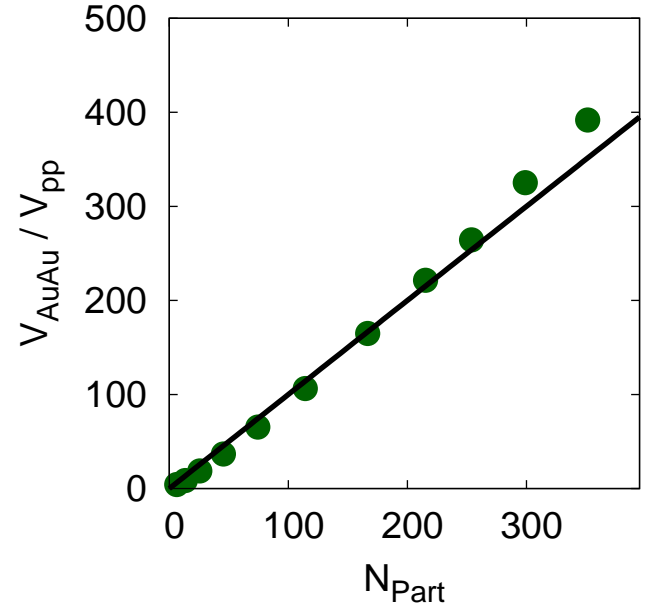


**Fig. 3.** (Color on-line) The system volume normalized to the volume in  $p + p$  collisions in 11 centrality classes in  $Au + Au$  collisions at  $\sqrt{s_{NN}}=200$  GeV as a function of the number of participants. Deviations from the  $N_{Part}$  scaling (straight line) are visible only in the central collisions.

at low beam energies, the Dalitz decay of  $\Delta$  resonances dominate the low mass region of the dilepton invariant mass spectrum (see e.g. [32–34]). Above mid SPS beam energies, however, the number of mesons exceed the num-

ber of baryons in heavy-ion collisions and at RHIC beam energies, the emission of dileptons from baryons is overwhelmed by orders of magnitude by the mesonic sources. Thus, we do not consider the dileptons stemming from decays of baryons in this work because the contribution is completely negligible at all invariant masses.

Hadron	direct	Dalitz	other
$\pi^0$	-	$\pi^0 \rightarrow \gamma e^+ e^-$	-
$\eta^0$	-	$\eta^0 \rightarrow \gamma e^+ e^-$	$\eta^0 \rightarrow \pi^+ \pi^- e^+ e^-$
$\eta'$	-	-	$\eta' \rightarrow \pi^+ \pi^- e^+ e^-$
$\rho^0$	$\rho^0 \rightarrow e^+ e^-$	-	-
$\omega^0$	$\omega^0 \rightarrow e^+ e^-$	-	$\omega^0 \rightarrow \pi^0 e^+ e^-$
$\phi^0$	$\phi^0 \rightarrow e^+ e^-$	-	$\phi^0 \rightarrow \eta e^+ e^-$
$J/\psi$	$J/\psi \rightarrow e^+ e^-$	$J/\psi \rightarrow \gamma e^+ e^-$	-
$\psi'$	$\psi' \rightarrow e^+ e^-$	$\psi' \rightarrow \gamma e^+ e^-$	-
$D$ mes.	-	-	$D^\pm \rightarrow e^\pm \nu_e + X$

**Table 1.** List of decay channels relevant for dielectron production in  $p + p$  collisions at  $\sqrt{s}=200$  GeV. For  $D^\pm$  mesons, 7 semileptonic (electron(positron) + anti-neutrino(neutrino) + 1 or 2 light hadrons) decay channels are considered. For the neutral ( $D^0$  and  $\bar{D}^0$ ) mesons and  $D_s^\pm$ , there are 6 semileptonic decay channels taken into account

The decay probability of a meson into a pair of leptons depends on the invariant mass of the lepton pair. A generic expression for the decay probability is known from Ref. [35]

$$\frac{d\Gamma^{X \rightarrow \gamma l^+ l^-}}{dM} = \frac{\Gamma^{X \rightarrow l^+ l^-}}{M} \frac{4\alpha}{3\pi} \sqrt{1 - \frac{4m_l^2}{M^2}} \times \left(1 + \frac{2m_l^2}{M^2}\right) \left(1 - \frac{M^2}{m_X^2}\right)^3 |F^{X \rightarrow \gamma \gamma}(M)|^2. \quad (2)$$

Here  $m_l$ ,  $m_X$  and  $M$  are the masses of the lepton, the decaying meson and the invariant mass of the dilepton pair, respectively. The form factors  $F^x(M)$  have been studied extensively both experimentally and within different models. In this work we have employed the form factors arising from the vector-meson dominance model considerations [4, 35]

$$F^{\eta \rightarrow \gamma \gamma}(M) = \left(1 - \frac{M^2}{(0.72\text{GeV})^2}\right)^{-1}$$

$$F^{\pi^0 \rightarrow \gamma \gamma}(M) = 1 + \frac{5.5}{\text{GeV}^2} M^2. \quad (3)$$

The  $\omega \rightarrow \pi^0 l^+ l^-$  channel is calculated from

$$\frac{d\Gamma^{\omega \rightarrow \pi^0 l^+ l^-}}{dM} = \frac{\Gamma^{\omega \rightarrow \pi^0 \gamma}}{M} \frac{2\alpha}{3\pi} \sqrt{1 - \frac{4m_l^2}{M^2}} \left(1 + \frac{2m_l^2}{M^2}\right) \times \left[\left(1 + \frac{M^2}{m_\omega^2 - m_\pi^2}\right)^2 - \frac{4m_\omega^2 M^2}{(m_\omega^2 - m_\pi^2)^2}\right]^{3/2} |F^{\omega \rightarrow \pi^0 l^+ l^-}(M)|^2$$

with the form factor

$$|F^{\omega \rightarrow \pi^0 l^+ l^-}(M)|^2 = \frac{(0.67\text{GeV})^4}{((0.67\text{GeV})^2 - M^2)^2 + (0.0516\text{GeV}^2)^2}. \quad (5)$$

The decay widths for the direct decays of vector mesons depend on the mass of the decaying resonance. In practice this matters for  $\rho^0$  direct decays only, since all other mesons are sufficiently narrow that the decay width can be considered constant. For the  $\rho^0$  direct decay, the decay width reads [36]

$$\Gamma^{V \rightarrow l^+ l^-}(M) = \frac{m_0^3}{M^3} \Gamma^{V \rightarrow l^+ l^-}(m_0) \quad (6)$$

in which  $M$  is the  $\rho$ -meson mass and  $m_0$  denotes the pole mass. The mass dependent branching fraction of the  $\rho^0$  meson into a pair of leptons is obtained from Eq. (6) by dividing it with the mass dependent total width of the  $\rho^0$  meson:

$$\Gamma_{tot}^{\rho^0}(M) \simeq \Gamma^{\rho \rightarrow \pi\pi} = \Gamma(m_0) \left(\frac{m_0}{M}\right)^2 \frac{(M^2 - 4m_\pi^2)^{3/2}}{(m_0^2 - 4m_\pi^2)^{3/2}}. \quad (7)$$

Above the  $\phi$  meson mass, the dilepton invariant mass spectrum attains contributions mainly from the decays of charmed hadrons. Radiative decays of  $J/\psi$ 's into dileptons have been studied in detail in [37]. Since it is not possible to (completely) disentangle the direct ( $J/\psi \rightarrow l^+ l^-$ ) and Dalitz decays ( $J/\psi \rightarrow \gamma l^+ l^-$ ) of  $J/\psi$  in the collision experiments, one needs to take into account also the Dalitz decay of  $J/\psi$  in the analysis. This will modify somewhat the shape of the invariant mass spectrum of the dileptons stemming from decays of charmonia. We have implemented the analytical formula [37]

$$\frac{d\Gamma^{X \rightarrow l^+ l^- \gamma}}{dM} = \frac{\alpha}{\pi} \frac{2M}{m_X^2 - M^2} \left(1 + \frac{M^4}{m_X^4}\right) \times \left(\ln \frac{1+r}{1-r} - r\right) \Gamma_0^{X \rightarrow l^+ l^-}, \quad (8)$$

which has been used successfully in describing the spectral shape of the radiative decays of  $J/\psi$  measured both in DESY as well as in PHENIX  $p + p$  collisions [1]. In Eq. (8)  $m_X$  is the mass of the decaying particle,  $M$  the invariant mass of the dilepton pair and  $r = \sqrt{1 - 4m_l/M^2}$ . This distribution diverges when  $E_\gamma \rightarrow 0$  ( $M \rightarrow m_X$ ) and thus a cut in energy must be introduced. A suitable value for the mass cut-off has been found [37] to be around  $E_{\min} \approx 10$  MeV, which we have also employed. Integrating Eq. (8) gives us the widths of the radiative charmonia decays:  $\Gamma^{J/\psi \rightarrow \gamma e^+ e^-} = 0.32 \Gamma^{J/\psi \rightarrow e^+ e^-}$  and  $\Gamma^{\psi' \rightarrow \gamma e^+ e^-} = 0.34 \Gamma^{\psi' \rightarrow e^+ e^-}$ . We have used these widths in evaluating the branching ratios for the charmonia Dalitz decays in our calculations. It is worth mentioning that our estimated branching fraction  $\text{BR}(J/\psi \rightarrow \gamma e^+ e^-)$  is about twice the value listed in the most recent PDG book [28]. However, our choice agrees somewhat better with the shape of the dielectron spectrum near the  $J/\psi$  peak than in the case of the PDG value for the  $J/\psi$  Dalitz decay branching ratio. The branching fraction for the  $\psi'$  Dalitz decay is not yet measured and thus a comparison is not possible.

For all other hadrons - not explicitly mentioned above - we have assumed a relativistic Breit-Wigner spectral function and the partial widths are then evaluated in a

simplified procedure taking into account only trivial mass threshold effects for the different decay channels to correct for the available phase space.

#### 4 Charmonium and continuum background of dileptons from heavy quark decays

The weak decays of  $D$  mesons  $D \rightarrow l + \nu_l + h$ , in which  $h$  denotes one or two non-charmed hadrons, constitute the main source of the "dilepton continuum" in the intermediate mass region at RHIC energies. At RHIC energies in proton-proton collisions, there is most often zero or a single charmed quark-anti-quark pair created. When this pair of charmed quarks hadronizes, the most likely result is that each of the charmed quarks end up in a  $D$  and  $\bar{D}$  meson. When the  $D$  mesons subsequently decay into leptons and hadrons, we may have an extra lepton pair stemming from the  $D$  meson decays in the final state. It is very difficult to subtract the leptons originating from the  $D$  meson decays in the collision experiments and thus the measured dilepton invariant mass spectrum usually includes this contribution. The contribution of the  $D$  meson decays is only significant far away from the true sources of dileptons and dominates the spectral shape between the 'peaks' of the  $\phi$  and  $J/\psi$  mesons. Thus, one needs to carefully consider the  $D$  mesons as dilepton emitting sources in high-energy collision experiments.

The slope of the dilepton continuum in the IMR arises as a superposition of the momentum distributions of the measured leptons coming from the individual  $D$  meson decays. Since the measurement is carried out at mid-rapidity and we are interested in invariant masses larger than 1 GeV, it is clear that the major contribution to the invariant mass of the dilepton continuum in the IMR arises from the transverse momenta of the decaying open charm mesons. Accordingly, it is important to model the transverse momentum spectrum of the  $D$  mesons more carefully than in the longitudinal direction, i.e. the rapidity distribution.

We will employ a very simple model to evaluate the rapidity distributions of charmed hadrons. Namely, we assume that all charmed quark-anti-quark pairs are produced via splitting of a hard gluon created in the initial hard collisions. We also assume that the hard gluons - from which all  $c\bar{c}$ -pairs originate - are created via gluon-gluon fusion processes in the initial hard scatterings of the gluons from the target and projectile. In this case, the final charmed hadron rapidity distributions will closely follow the rapidity distribution of the hard gluons emitted in the collision experiment.

In order to fix the rapidity distributions of charmed hadrons we harness the idea of limiting fragmentation [38], which has been verified experimentally at ultra-relativistic beam energies both in hadron-hadron [39,40] as well as in heavy-ion collisions [41]. Let us consider a collision of two gluons with momentum fractions of  $x_1$  and  $x_2$  of the colliding projectile and target. One can show (see e.g. [42]) that the resulting parton rapidity distribution at large momentum fraction (i.e.  $x_1 \gg x_2$  or vice versa) is proportional

to the parton distribution function itself

$$\frac{dN}{dy} \sim x_1 g(x_1) \quad ; \quad x_1 = \frac{p_T}{m_N} e^{y-y_{\text{beam}}} \quad (9)$$

and is approximately independent on the  $Q^2$  scale due to Bjorken scaling. In Eq. (9)  $p_T$  and  $y$  are the transverse momentum and rapidity of the produced gluon,  $m_N$  is the mass of the beam particle (in this case the proton). Thus, in order to estimate the rapidity distribution of the charmed hadrons, we have to adopt a suitable parametrization for the parton distribution function in Eq. (9). We have chosen the following NNLO pQCD best fit parametrization from Ref. [43] for our gluon distribution

$$xg(x) \sim x^a (1-x)^b (1 + \gamma_1 \sqrt{x} + \gamma_2 x) \quad \text{with} \\ a = -0.118 \quad b = 9.6 \quad \gamma_1 = -3.83 \quad \text{and} \quad \gamma_2 = 8.4. \quad (10)$$

This parametrization is given at  $Q^2=9 \text{ GeV}^2 \approx M_{J/\psi}^2$  and we approximate the gluon distributions at higher  $Q^2$  with the same parametrization.

We can now evaluate the rapidity distribution of charmed hadrons with a modified Brodsky-Gunion-Kuhn (BGK) model [44] introduced in Ref. [45], in which the parton number density of produced partons along the beam axis is proportional to a triangle defined by the momentum fractions  $x_1$  and  $x_2$  as follows: The center of mass of the colliding partons move with rapidity  $y_{cm} = \text{atanh}(\frac{x_1-x_2}{x_1+x_2})$ . We assume that the probability along the rapidity axis to find the hard gluon - fragmenting into a charmed quark pair - is defined by a triangle whose maximum is at  $y_{cm}$  and which goes linearly to zero at  $y = \text{asinh}(x_1 \sqrt{s}/2m_N)$  and  $y = -\text{asinh}(x_2 \sqrt{s}/2m_N)$ . The area of this triangle is set to unity so that it represents a proper probability.

We have estimated the charmonium cross sections by the expression (taken from Ref. [23])

$$\sigma_i^{NN}(s) = f_i a \left(1 - \frac{m_i}{\sqrt{s}}\right)^\alpha \left(\frac{\sqrt{s}}{m_i}\right)^\beta \theta(\sqrt{s} - \sqrt{s_{0i}}) \quad (11)$$

in which  $\sqrt{s}$  is the center-of-mass collision energy (per nucleon pair) and  $m_i$  is the mass of the charmonium state  $i$ . The parameters  $\alpha=10$ ,  $\beta=0.775$  and  $a$  are common for all charmonia and fitted to experimental data. The threshold factors read  $\sqrt{s_{0i}} = m_i + 2m_N$  while the parameters  $f_i$  were fitted separately in [23] for each of the states ( $f_i=0.636$ ,  $0.581$  and  $0.21$  for  $\chi_c$ ,  $J/\psi$  and  $\psi'$ , respectively). Above, the multiplicity label  $\chi_c$  denotes the sum of the three  $\chi_{0c}$ ,  $\chi_{1c}$  and  $\chi_{2c}$  states. All these states decay into  $J/\psi$  and we have taken the sum of their branching ratios (0.55) into  $J/\psi$  as our branching ratio for the generic " $\chi_c$ ". We have slightly re-adjusted the common normalization factor  $a$  from 0.16 mb to 0.133 mb in order to reproduce exactly the total  $J/\psi$  production cross section  $\sigma_{J/\psi}^{NN} = 3.0 \mu\text{b}$  measured by the PHENIX collaboration [46]. The rapidity distribution of  $J/\psi$ 's in proton-proton collisions at  $\sqrt{s}=200$  GeV, evaluated according to Eqs. (9), (10) and (11) is compared with the PHENIX measurement in Fig. 4. The agreement appears good enough so that we can estimate both the rapidity

density at mid-rapidity as well as the total cross section in our simple model.

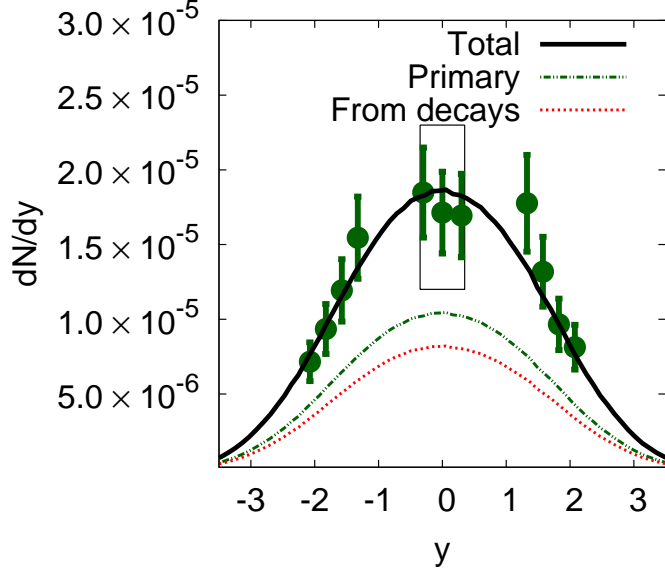


**Fig. 4.** (Color on-line) Calculated and measured  $J/\psi$  rapidity distribution in proton-proton collisions at  $\sqrt{s}=200$  GeV. The data (full dots with error bars) are from the PHENIX collaboration [46]. The primary production of  $J/\psi$ ,  $\chi_c$  and  $\psi'$  are evaluated as described in the text. The "From decays" - line denotes the feeding from  $\psi'$  and  $\chi_c$  states. The central rapidity region, in which the dilepton measurement is carried out, is indicated by the vertical lines.

The reason we have taken the trouble to set up a model that can describe the  $J/\psi$  rapidity distribution in  $p + p$  collisions is that we need this model to evaluate the rapidity distribution of  $D$  mesons. The open charm rapidity distribution is not yet measured at this beam energy and thus we need to calculate it. Since we have seen that our model can describe the  $J/\psi$  data in this collision system, we can fairly safely assume that the same model will, at least approximately, describe the longitudinal part of the open charm momentum distribution as well.

Let us turn our attention to the transverse directions now. As we discussed earlier, the transverse direction contributes most to the invariant mass of the dileptons from open charm decays at mid-rapidity. This is why we will rely on experimental data here. The transverse momentum distributions of  $D$  mesons are experimentally not well known, though. What is much better known is the rapidity and transverse mass distribution of  $J/\psi$ 's in proton-proton collisions at RHIC. We deem that the momentum distributions of  $D$  mesons resemble the corresponding ones for  $J/\psi$  since the shape of the distribution - especially in the beam direction - should be primarily determined by the dynamics of the hadronizing charmed quarks. Thus, we assume that the  $D$  meson transverse momentum distribution has a similar form as that for  $J/\psi$ 's in the same collision system. The  $p_T$  spectrum of  $J/\psi$  [46,47] (measured by the PHENIX collaboration) can be described well

with the power-law function

$$\frac{dN}{dp_T} \sim (1 + (p_T/B)^2)^n, \quad (12)$$

see Figure 5. Here we have used the published data and fitted  $B=3.74$  and  $n=5.11$ .

According to our best knowledge, the transverse momentum distribution of  $D$  mesons have not been measured in proton-proton collisions at RHIC beam energies. Preliminary data [48] in  $Cu + Cu$  collisions do exist as well as already published data [49,50] in  $d + Au$  collisions at  $\sqrt{s_{NN}}=200$  GeV. The transverse momentum spectra of  $D$  mesons in these collision systems - divided by the number of binary collisions - along the corresponding  $J/\psi$  data in  $p+p$  collisions are shown in Fig. 5. The lines shown have the functional form of Eq. (12) and are fitted to the data. The  $D$  meson data do not allow to reliably fit both  $B$  and  $n$  (as well as the normalization) and so we have chosen to fix the parameter  $B = 3.74$  as in the case of  $J/\psi$  and re-fitted  $n = 10.7$  in order to describe the STAR data for  $d + Au$  collisions.

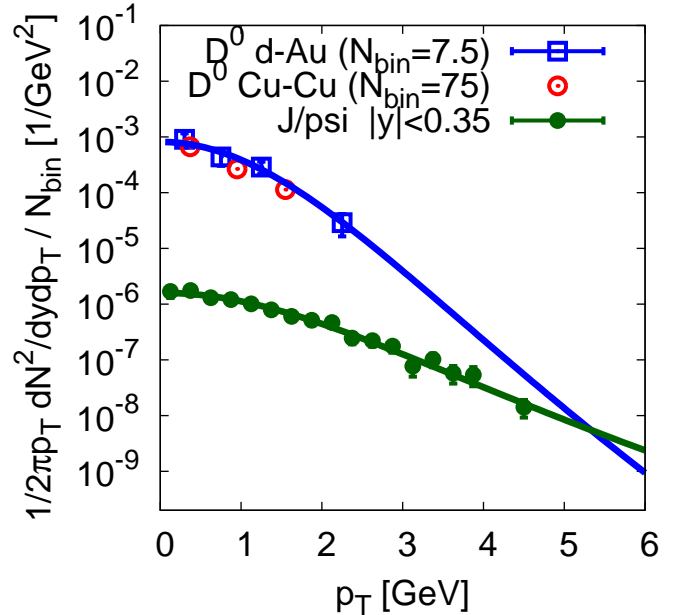


**Fig. 5.** (Color on-line)  $D$  meson  $p_T$  spectra per binary collision in  $d + Au$  [49] and  $Cu + Cu$  [48] collisions as well as the  $J/\psi$   $p_T$  spectrum [46] in  $p + p$  collisions. The lines are power-law fits to the data as described in the text.

The dilepton continuum stemming from  $D$  meson decays attains an extra feature compared with the dilepton emission from other sources. Namely, since the electron and positron are emitted by two different hadrons, the angular correlation as well as re-scattering effects can strongly alter the invariant mass spectrum of the final state dileptons. We assume here that the emitted leptons themselves always escape the collision zone unscathed and (re-)scattering effects can only take place on the hadronic

level. The angular correlations of the open charm hadrons are experimentally not well known and thus we will employ theoretical estimates.

We deem that the two charmed quarks are always emitted in  $180^\circ$  angle in their respective center-of-mass frame while this angle is typically much smaller in the laboratory frame due to large Lorentz boosts in the longitudinal direction, especially at large forward and backward rapidities. We assume here that the longitudinal direction is not different from the transverse directions in the CM frame of the fragmenting  $c\bar{c}$ -pair, i.e. that Eq. (12) describes the joint distribution of any two momentum components " $p_T$ " =  $\sqrt{p_x^2 + p_y^2}$  =  $\sqrt{p_x^2 + p_z^2}$  =  $\sqrt{p_y^2 + p_z^2}$  in the CM frame of the charmed hadrons. The angular distribution among the produced  $D$  mesons is then taken exactly back-to-back correlated in their respective CM frame and we need to boost the momenta of the produced  $D$  mesons into the laboratory frame in order to evaluate the angular correlations in that particular frame. We have cross-checked our approach and verified that our angular correlations - evaluated as described above - agree well with correlations evaluated with the PYTHIA [51] event generator. Alternatively, we might also have adopted the angular correlations from the PYTHIA simulations.

We have taken into account the 12 lightest  $D$  meson states ( $D^\pm$ ,  $D^{*\pm}$ ,  $D^0$ ,  $\bar{D}^0$ ,  $D^{*0}$ ,  $\bar{D}^{*0}$ ,  $D_s^\pm$  and  $D_s^{*\pm}$ ) all of whose mass is around 2 GeV. We have assumed that the relative primary multiplicity of these 12 states is determined purely by their spin -degeneracy while the total number of them is taken from the parametrization of Ref. [23]. On top of this, we have taken into account the empirical fact that in a jet fragmentation process, hadrons that include a strange or anti-strange quark suffer further suppression. We have used the canonical value 0.3 for such a strangeness suppression factor for the  $D_s$  and  $D_s^*$  states in our analysis as in Ref. [23] which stems from PYTHIA calculations. One should not confuse this factor with the  $\gamma_S$  parameter included in the thermal model analysis. The factor 0.3 here concerns the hard scatterings only, while the  $\gamma_S$  parameter takes into account also some of the soft physics on top of the suppression on the hard scattering level.

The kinematics of the decays of the excited  $D$  mesons can be neglected because of the small mass difference between the  $D^*$  and  $D$  states. In each of the cases, the excited state relaxes itself by emitting a very soft pion and thus the daughter  $D$  inherits practically the momentum of the decaying parent state. We deem that by properly considering all of the lightest  $D$  mesons (and their relative abundances), we can then hope to extract the total charm production cross section in our analysis. Alternatively we could have just included the lowest lying  $D$  meson states, since these are the only ones decaying into leptons, but in this case the normalization factor, the number of final state  $D$  mesons would not have a clear physical interpretation as a cross section. Rather than taking the rapidity densities of different charmed hadrons at mid-rapidity as free parameters, we wish to estimate the total cross sections of the different states and suitably distribute the

produced charmed hadrons at different rapidities. In order to estimate the rapidity density of  $D$  mesons around mid-rapidity, we take the total cross section for open charm production<sup>2</sup> from the parametrization given in [23] and distribute these along rapidity as described earlier.

## 5 Results for dileptons

### 5.1 Proton-proton collisions

Let us first look at the proton-proton collisions. Our calculated dielectron yields are compared with the experimental data in Fig. 6. The top panel of Figure 6 shows the low mass region where the emission is dominated by the decays of light mesons. One can see that the spectrum can be reproduced very well within the statistical hadronization ansatz described in the previous sections. We mention that the  $p + p$  dilepton mass spectra are also well reproduced within the HSD transport approach [5] where the charm production and angular correlations have been evaluated within PYTHIA.

The shapes of the two peaks arising from the direct decays of  $\omega$  and  $\phi$  mesons are essentially determined by the experimental mass resolution. The natural width of these peaks would be only about 8 and 4 MeV, respectively. The mass resolution of the experiments, however, exceeds the vacuum width of these hadrons and thus we have taken this into account by smearing the peaks according to Gaussian distributions with a width corresponding to an experimental mass resolution of 10 MeV for the light mesons except for the  $\phi$ -meson direct decay whose resolution was taken to be 8.1 MeV [52]. The mass resolution of dielectrons from the charmed hadron decays was taken to be 2% of  $m_{e^+e^-}$ . By doing so, especially the shape of the  $\phi$  meson peak is strongly modified and becomes compatible with the experimental data as seen in Fig. 6. We have not considered in-medium modifications of the spectral functions in this work and thus any apparent change in the vacuum spectral functions is solely due to experimental acceptance cuts.

We find no discrepancy<sup>3</sup> between the data and our model in the low invariant mass region and can conclude that the data are very well described within the statistical hadronization model assuming a thermalized fireball. The only non-equilibrium feature we have taken into account here is the strangeness suppression factor  $\gamma_S$ . By this factor we introduce a new - partly free but correlated - normalization for hadrons consisting of one or more

<sup>2</sup>  $\sigma_{c\bar{c}} = \sigma_{D^+} + \sigma_{D^0} + \sigma_{D_s} + \sigma_{D^{*+}} + \sigma_{D^{*0}} + \sigma_{D_s^*} = 485 \mu b$

<sup>3</sup> The invariant mass region between the  $\omega$  and  $\phi$  meson peaks is somewhat under-estimated in our approach. We deem that this is due to our approximation that the angular correlations among the  $D$  mesons are back-to-back in the center-of-mass frame. In reality, a backward peaked but narrow angular distribution is expected, which softens the spectrum somewhat and populates the low invariant mass region. This effect, however, would be only visible in the region between the  $\omega$  and  $\phi$  mesons.



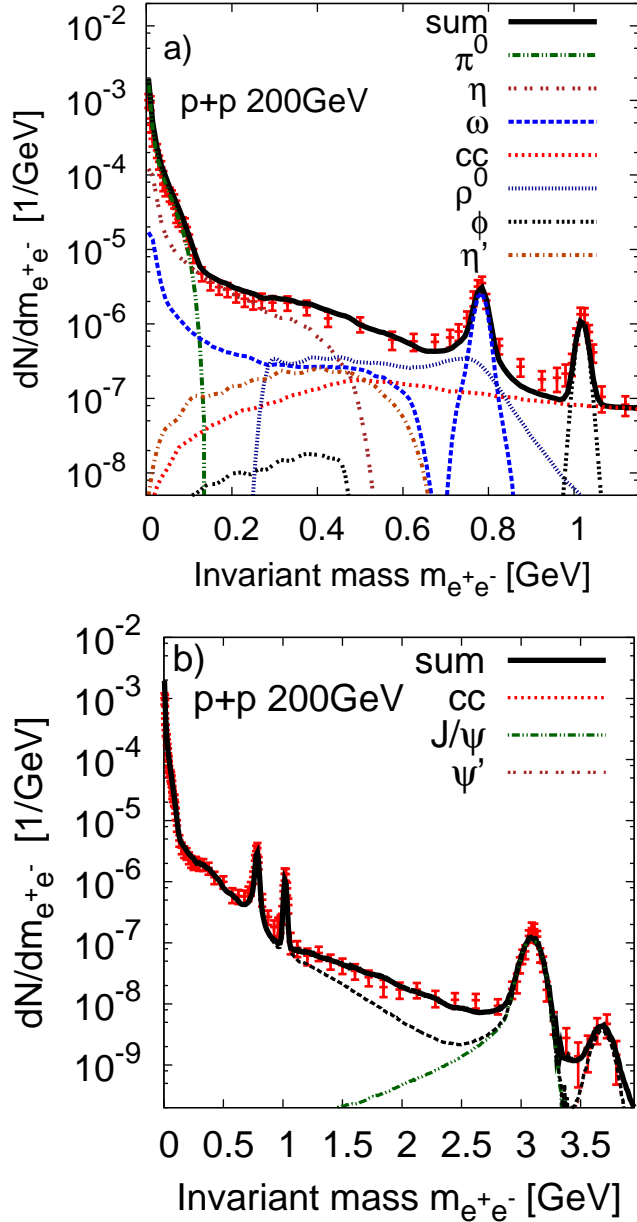


**Fig. 6.** (Color on-line) Invariant mass spectrum of pairs of electrons and positrons in proton-proton collisions at  $\sqrt{s} = 200$  GeV. The data are from the PHENIX collaboration [1] while the contribution from different dilepton emitting sources are calculated as explained in the text. The full thick black line denotes the sum from all relevant sources. The LMR is shown in the upper panel while the whole invariant mass range is shown in the bottom panel.

strange quarks. In practice, the action of the  $\gamma_S$  parameter is best visible in the  $\phi$  meson peak. Since there are no resonances decaying into the  $\phi$  meson the sole rapidity density of the  $\phi$  meson is calculated according to Eq. (1). With our choice for the value of  $\gamma_S$  the  $\phi$  meson rapidity density is multiplied by a factor  $\gamma_S^2 = 0.36$ . Obviously, without this extra strangeness suppression the production of dileptons from the decays of  $\phi$  mesons would be dramatically

over-estimated. The  $\gamma_S$  parameter affects also the yields of  $\eta$  and  $\eta'$  mesons, whose primary thermal production rates are multiplied by  $\gamma_S$  in order to take into account the fact that these mesons are considered to carry "hidden strangeness". Thus the value of  $\gamma_S$  is mostly (but not solely) determined by the  $\phi$  meson. We remind the reader here that, besides the overall normalization, we have not fine tuned any of the thermal parameters in this work, instead, we have used the values fitted in Ref. [27] to STAR data.

The whole invariant mass spectrum is shown in the lower panel of Figure 6. Let us look at the IMR between the  $\phi$  and  $J/\psi$  peaks now. The solid and dashed black lines are evaluated as explained in the last Section implementing the transverse momentum profile fitted to the  $D$  meson transverse momentum spectrum in  $d + Au$  collisions. The only difference between these two lines is that the upper solid line is evaluated assuming back-to-back angular correlations in the center-of-mass frame between the two fragmenting  $D$  mesons while the lower dashed line is the same with random correlations. From the figure it is clear that the model with random correlations does not describe the IMR spectrum properly for  $p + p$  reactions.

From this we can conclude, in accordance with the original PHENIX publication [1], that a model with strong correlations (no final state interactions) among the produced  $D$  mesons seems to be favored by the data over the random correlation in case of proton-proton collisions. We mention that in the extreme case of exact back-to-back correlations in the laboratory frame among the  $D$  mesons, the slope of the dilepton continuum in the IMR is reproduced but in this case too few dileptons are emitted in the LMR. We do not explicitly show these results but note that the continuum between the  $\omega$  and  $\phi$  would be under-estimated by about an order of magnitude in this over-simplified scenario.

We may conclude that once all relevant kinematical as well as acceptance effects are taken into account, the electron-positron invariant mass spectrum can be understood very well in both the LMR and IMR in proton-proton collisions within our simple model and parametrization. This will serve as a baseline for our comparative analysis in heavy-ion collisions for different centralities. We mention in passing that the dilepton mass spectra from our simplified model agree with those from the HSD approach [5] on the 20% level when using vacuum spectral functions for the hadrons in the transport approach.

## 5.2 Heavy-ion collisions

Let us turn to heavy-ion collisions now. We have seen in the previous Section that the dilepton invariant mass spectrum can be well understood in proton-proton collisions and we will now try to extrapolate our results from  $p + p$  collisions to heavy-ion collisions to identify the magnitude of possible additional production channels from partonic sources as suggested e.g. in Ref. [53] for SPS energies.

The non-charmed hadron yields are expected to scale with the participant number ( $N_{\text{Part}}$ ) when comparing  $p + p$

and heavy-ion collisions while - assuming that the charmed quark pairs are created solely in the initial hard scatterings - the number of binary collisions ( $N_{\text{bin}}$ ) should be the correct scaling variable for the charm sector. Both  $N_{\text{Part}}$  and  $N_{\text{bin}}$  can be estimated within the Glauber model and are conventionally used also in the experimental analyses. We have used the same values for  $N_{\text{Part}}$  and  $N_{\text{bin}}$  [31, 54] that are employed by the experiments at RHIC in order to be consistent with similar previous analyses.

### 5.2.1 Low invariant mass region

The  $Au + Au$  and  $Cu + Cu$  collisions are treated different in this paper. For the  $Au + Au$  collisions we have fitted the width of the clusters' transverse momentum distribution and the system volume to the PHENIX data, see Figures 2 and 3, and evaluated the dilepton invariant mass spectrum in  $Au + Au$  collisions implementing the 'optimized' parameters. Detailed measurements of identified hadron transverse momentum spectra are not yet available in the  $Cu + Cu$  collisions and thus we have evaluated the yields of dielectrons in the LMR in  $Cu + Cu$  collisions such that we use the transverse momentum profile fitted to the  $Au + Au$  collisions also in  $Cu + Cu$  collisions at the same  $N_{\text{Part}}$ . The volume in  $Cu + Cu$  collisions at different centralities is evaluated by scaling the system volume in  $p + p$  collisions with the number of participants. As one can see from the Figure 3, the fitted volumes scale with  $N_{\text{Part}}$  in the  $Au + Au$  collisions in the  $N_{\text{Part}}$  region relevant for  $Cu + Cu$  collisions and thus we deem that the  $N_{\text{Part}}$  scaling should be a good approximation in the  $Cu + Cu$  case, at least in the non-central collisions.

We have evaluated the dilepton yields in  $Au + Au$  and  $Cu + Cu$  collisions as described above, see Figs. 7 and 8. In the lower panel of Fig. 7 we show our results together with the experimental data [55] in minimum bias  $Au + Au$  collisions in the whole invariant mass range while in the top panel a zoom to the LMR is presented. In Fig. 8 the experimental results from Refs. [2, 56] in different centrality bins both in  $Au + Au$  (top panel) and  $Cu + Cu$  (bottom panel) collisions are shown. The  $Cu + Cu$  data in different centrality bins are still preliminary and the error bars are not yet available.

In the following we will concentrate on discussing the  $Au + Au$  collisions. Essentially the same conclusions will, however, hold also for the  $Cu + Cu$  collisions. Let us take a closer look at the LMR first. From the top panel of Fig. 8 one can see that the data can be described well in the most peripheral centrality bin in  $Au + Au$  collisions in the LMR. This centrality class is special among the centrality classes in  $Au + Au$  collisions because in all other centrality classes the relative strangeness production is found to be nearly in chemical equilibrium with  $\gamma_S \approx 1$  [19]. We have taken the increase in relative strangeness production into account in our analysis by setting the  $\gamma_S$  parameter to unity in every other centrality bins except in the most peripheral collisions, i.e. in the centrality bin labeled with "5" in Fig. 8a and "4" in Fig. 8b. The results with both  $\gamma_S = 0.6$  (solid) as well as  $\gamma_S = 1$  (dashed) are shown for the

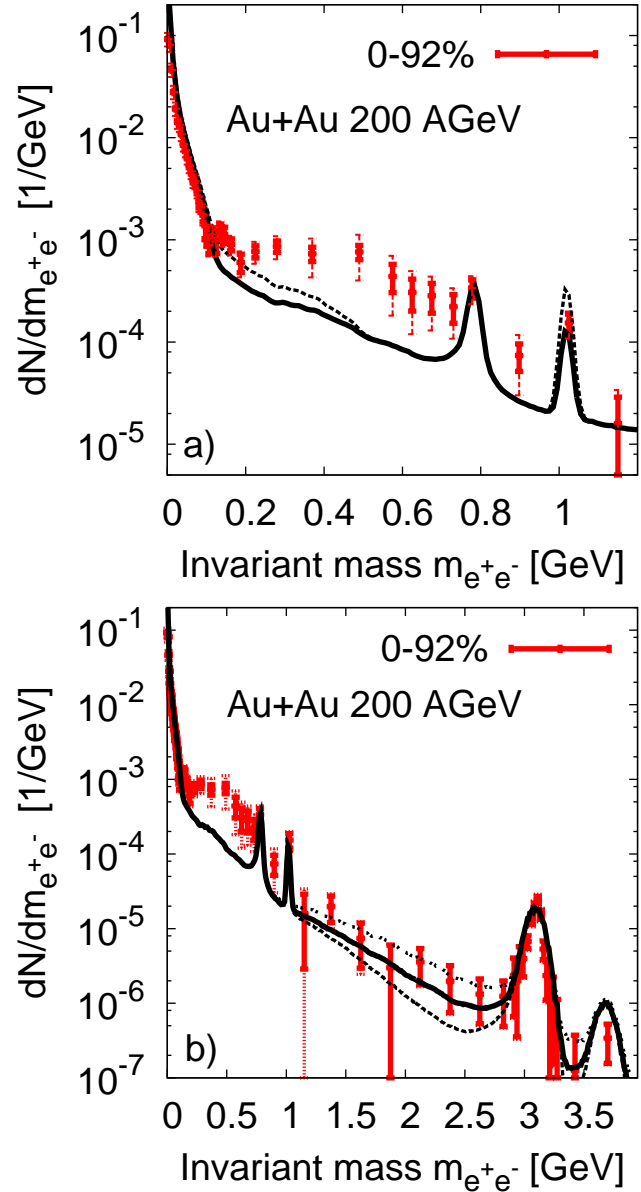


**Fig. 7.** (Color on-line) Invariant mass spectrum of pairs of electrons and positrons in minimum bias  $Au + Au$  collisions at  $\sqrt{s_{\text{NN}}}=200$  GeV [55] compared with model calculations. The low invariant mass region is shown in the top panel while the results in the full invariant mass region are shown in the bottom panel. The solid line indicates the model results scaled from  $p + p$  collisions such that the charmed hadron yields are scaled with the number of binary collisions  $N_{\text{bin}}$  while the non-charmed hadron yields are scaled with  $110 V_{\text{pp}}$  (the volume in  $p + p$  collisions). The dashed curve (bottom panel) indicates the results scaled from  $p + p$  collisions assuming a random correlation among the  $D$  mesons. The calculation with the  $\gamma_S$  parameter set to unity is indicated by the dashed line (top panel) slightly above the solid one in the LMR. The dotted curve (bottom panel) indicates the results evaluated with angular correlations kept the same as in  $p + p$  collisions. The solid and dotted error bars stand for the statistical and statistical + systematic errors added in quadrature, respectively.

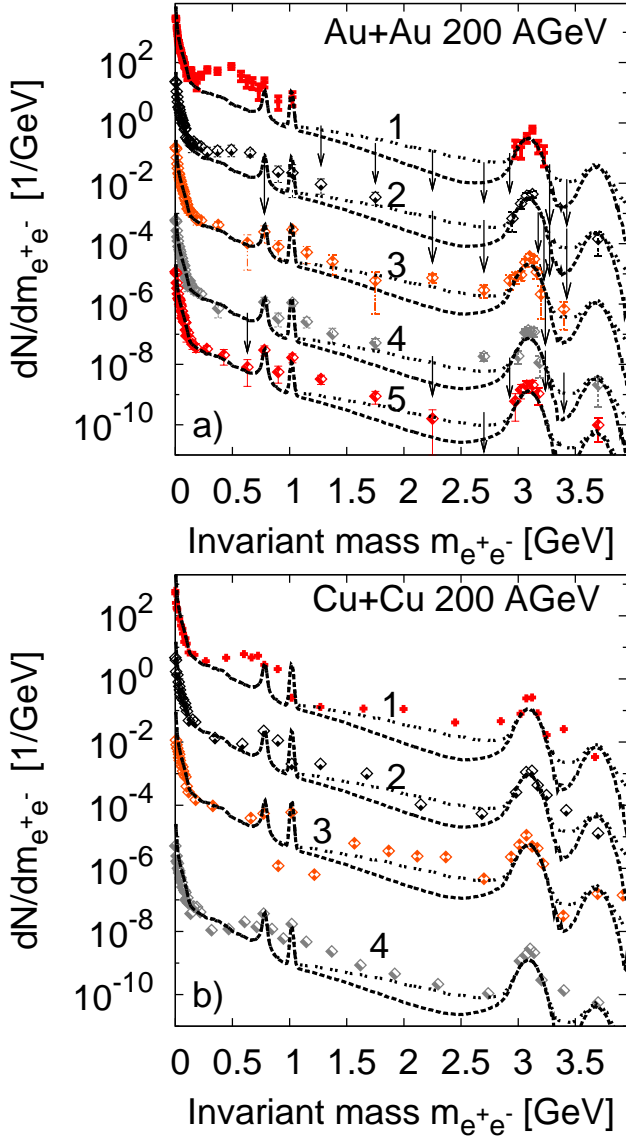


**Fig. 8.** (Color on-line) Invariant mass spectrum of pairs of electrons and positrons in  $Au + Au$  (top) [2] and  $Cu + Cu$  (bottom) [56] collisions at  $\sqrt{s_{NN}} = 200$  GeV in different centrality classes compared with the model calculations. The centrality bins are labeled from central to peripheral as 1 (0-10%), 2 (10-20%), 3 (20-40%). Centrality bin 4 consist on (40-94%) and (40-60%) most central events in  $Cu + Cu$  and  $Au + Au$  collisions, respectively, while the centrality bin 5 includes (60-92%) most central collisions. Both the data and model calculational results are scaled with factors of  $10^4$  (0-10%),  $10^2$  (10-20%), 1 (20-40%),  $10^{-2}$  (40-60%) as well as  $10^{-3}$  (60-92%) and (40-94%) for clarity. The double dotted lines indicate the model results scaled from  $p + p$  collisions such that the charmed hadron yields are scaled with  $N_{bin}$ . The non-charmed hadron yields are scaled with  $N_{Part}$  in the case of  $Cu + Cu$  collisions while in  $Au + Au$  collisions we have scaled the yields with the fitted volumes. The dashed lines indicate the results scaled from  $p + p$  collisions with random correlations among the open charm hadrons. The starting point of the downward pointing arrows denote the data points which are defined as upper limits only.

minimum bias  $Au + Au$  collisions in the top panel of Figure 7. One can see that the increase in relative strangeness production as a function of centrality is not strong enough to explain the excess in the LMR in minimum bias  $Au + Au$  collisions.

From Figure 8, one can see that the LMR data in  $Au + Au$  collisions in peripheral and in semi-central bins can be reasonably well described within the statistical hadronization model. On the other hand, in the two most central bins as well as in the minimum bias collisions the increase in strangeness production can not explain the excess of dileptons in the low invariant mass region from 0.15 to 0.6 GeV. In  $Cu + Cu$  collisions, it seems that there is significant excess in the LMR over the hadronic cocktail only in the most central collision bin while the LMR is fairly well described for the other centralities.

We have, furthermore, studied the effect of the transverse flow on the dielectron invariant mass spectrum in  $Au + Au$  collisions by comparing the results evaluated with the maximum and minimum width for the clusters' transverse momentum distribution. The largest (see Fig. 2) width,  $\sigma_{p_T} = 13.5$  GeV, was fitted in (15-20%) most central collisions while for the  $p + p$  and (60-92%) most central collisions we use  $\sigma_{p_T} = 10.0$  GeV. We have evaluated the dielectron invariant mass spectrum with these two widths keeping all their parameters fixed ( $T = 170$  MeV,  $V = V_{pp}$  and  $\gamma_S = 1$ ) and calculated the ratio of the resulting invariant mass spectra of dielectrons in the PHENIX acceptance, see Figure 9.

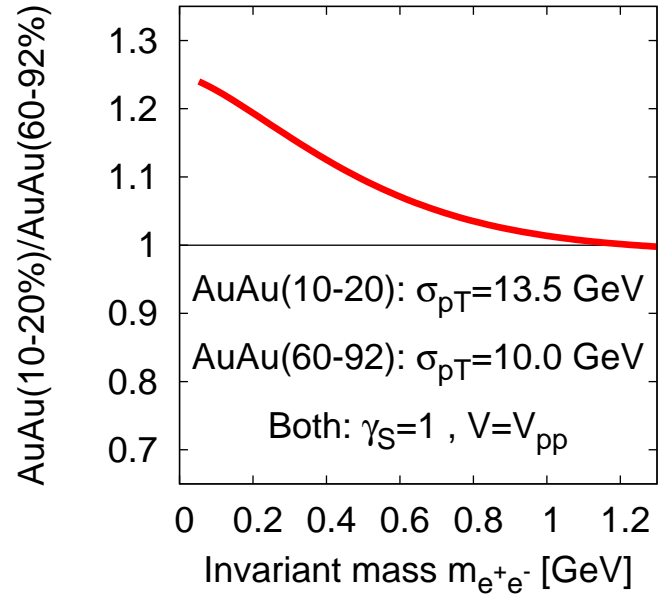


**Fig. 9.** (Color on-line) Ratio of invariant mass spectrum of electron-positron pairs within the PHENIX acceptance evaluated with two different transverse flow profiles keeping other parameters fixed.

As expected, the increase in the transverse flow enhances the dielectron yields in the PHENIX acceptance especially at very low invariant masses while above the  $\omega$

meson peak equal amounts of dileptons hit the PHENIX acceptance with both transverse flow profiles. In general the effect is moderate and the increase in flow can increase the dielectron yields up to 30% in the  $\pi^0$  region, much less than the observed excess by factors up to 4-5. Thus, one can conclude that the broadening of transverse momentum distributions as a function of centrality plays only a minor role in the dielectron radiation from the decays of light hadrons.

### 5.2.2 Further correlated sources in the LMR

Besides the decays of light mesons, there are other correlated sources for dielectron production in high-energy nuclear collisions. In this Section, we will address some but not all of such processes. The contribution from most of these channels is very small and thus we concentrate here on the dominant channels, only. These additional channels, similarly to the the  $D$  meson case, arise in correlated decays of light hadrons that do not directly decay into electrons but produce single electrons via intermediate hadrons. An example of such a process is the  $\phi$ -meson decay  $\phi \rightarrow K^+K^-$ . The  $\phi$  meson has a long lifetime and a small hadronic cross section and thus many of the  $\phi$  meson decays take place outside the fireball. Now it can happen that the kaons from the  $\phi$  meson undergo semileptonic decays like  $K^+ \rightarrow \pi^0 e^+ \nu_e$  and charge conjugate for the  $K^-$ . If the  $\phi$  meson decays outside the fireball, the correlations are preserved and the experiment measures essentially additional correlated dielectron radiation from the  $\phi$  meson which survives the experimental subtraction procedure from uncorrelated  $e^+e^-$  decays.

Unlike the  $\phi$  meson, most of the short living resonances are expected to decay inside the fireball thus destroying the correlated signal. However, some of the interactions do take place in the dilute corona of the fireball in which case the correlated signal can be preserved even in central heavy-ion collisions. We do not perform a precise calculation for these correlations and make an estimate for the relative magnitude of core and corona emission, instead. Our results thus have to be considered as an upper limit estimate for a correlated background emission.

We have considered this type of correlated dielectron radiation from a selection of fairly light strange and neutral hadrons whose branching fractions into  $K\bar{K}$  are sizeable and reasonably well known. The additional channels we have studied in this work are listed in Table 2. We consider the kaonic channels only in this work, even though most of the processes could proceed via the  $\pi\pi$  channel as well. The pionic channels are found to be sub-leading compared to the kaonic channels and thus we have omitted pionic channels in this work.

We have considered all  $K^0$ 's as fixed 50% - 50% mixtures of  $K_S^0$  and  $K_L^0$  states and ignored the time dependent neutral kaon oscillations. Making a distinction between the long and short living states is important since the  $K_L^0$  has roughly a factor of 100 larger probability to decay semileptonically than the  $K_S^0$ . Electrons and positrons stemming from  $K_L^0$  decays are taken into account only if

Hadron			
$f_0(980)$	$K^+K^-$	$K^0\bar{K}^0$	-
$f_1(1285)$	-	-	$K\bar{K}\pi$
$f_2(1270)$	$K^+K^-$	$K^0\bar{K}^0$	-
$f'_0(1350)$	$K^+K^-$	$K^0\bar{K}^0$	-
$f'_1(1420)$	$K^{*+}K^- + c.c$	$K^{*0}K^0 + c.c$	-
$f'_2(1525)$	$K^+K^-$	$K^0\bar{K}^0$	-
$f_0(1500)$	$K^+K^-$	$K^0\bar{K}^0$	-
$f_1(1510)$	$K^{*+}K^- + c.c$	$K^{*0}K^0 + c.c$	-
$f_2(1430)$	$K^+K^-$	$K^0\bar{K}^0$	-
$\phi$	$K^+K^-$	$K^0\bar{K}^0$	-
$a_0^0(980)$	$K^+K^-$	$K^0\bar{K}^0$	-
$K(892)^\pm$	$K^\pm\pi^0$	-	-
$K(892)^0$	$K^0\pi^0$	-	-

**Table 2.** List of additional decay channels relevant for dielectron production in high-energy collision systems.

the  $K_L^0$  has decayed before the first detector (2 meters from the primary vertex) which reduces significantly the di-electron yields from the  $K^0$  decays.

The contributions from the additional correlated channels in (0-10%) most central  $Au + Au$  collisions are shown in top panel of Figure 10. We have added some of the channels in Figure 10 for clarity. The  $K^*$  denotes the sum of  $K^{*\pm}$ ,  $K^{*0}$  and  $K^{*-0}$  while  $f_{012}$  is the sum of  $f_0$ ,  $f_1$  and  $f_2$  and similarly  $f'_{012}$  denotes the sum of the  $f_0(1370)$ ,  $f_1(1420)$  and  $f_2(1525)$ . The contribution from the  $f_0(1500)$  is small and is not shown. For comparison, also the hadronic cocktail contribution from  $\eta$  and  $\rho^0$  mesons are shown by the thick solid lines. One can see that the correlated channels might indeed give a sizeable contribution to the dielectron invariant mass spectrum in the low invariant mass region and might even over-shine the standard hadronic cocktail emission precisely in the invariant mass region where the large excess was measured by PHENIX in central nucleus-nucleus collisions.

In the bottom panel of Figure 10 the standard hadronic cocktail result (solid) and the cocktail + additional correlated emission (dashed) are compared with the PHENIX data in the most central bin. Our results show that the correlated background from the exotic mesonic states may result in a large enhancement of the dielectron yields in the LMR, although re-scattering effects could significantly alter the results at least for some of the correlated channels. The sizeable contribution - relative to proton-proton reactions - is due to a factor  $\gamma_S^2$  which increases roughly by a factor of three from peripheral to central nucleus-nucleus collisions. Note, however, that we have addressed upper limits, only, and that a decorrelation by interactions in the hot medium is expected. Nevertheless, even our upper limit is clearly below the PHENIX signal for central nucleus-nucleus collisions and we may conclude that the additional channels considered here should not be responsible for the dilepton excess seen experimentally.

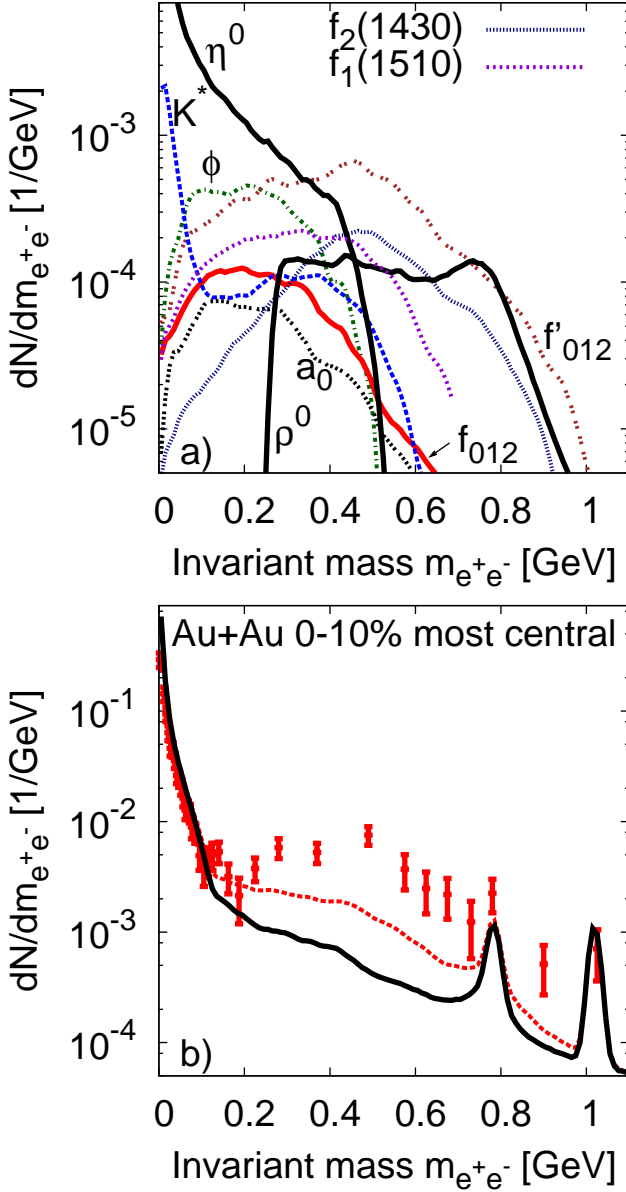


**Fig. 10.** (Color on-line) The upper limits for the invariant mass spectrum of pairs of electrons and positrons in (0-10%) most central  $Au + Au$  collisions arising from various correlated sources (top panel) in comparison with the PHENIX data and the standard cocktail calculation (bottom panel).

### 5.2.3 Intermediate mass region

We have estimated the charmed hadron yields in heavy-ion collisions by multiplying the corresponding yields in proton-proton collisions with the number of binary collisions for the contributions from charm mesons. This procedure should hold for open charm hadrons but actually we know that the production of charmonium states suffer suppression in the hot and dense environment of partonic and hadronic nature. This suppression is usually expressed by the ratio  $R_{AA} = \frac{dN_{\psi}^{AA}}{N_{bin}dN_{\psi}^{pp}}$  which parametrizes the deviation from the simple  $N_{bin}$  scaling. PHENIX has mea-

sured this quantity for  $J/\psi$ 's both in  $Au + Au$  [57] as well as in  $Cu + Cu$  [58] collisions. So far there is no fully convincing model calculation that explains the observed  $R_{AA}$  on a satisfactory level and thus we have taken the simplest approach and assumed that  $R_{AA}$  is a linear function<sup>4</sup> of centrality. This approximation seems to hold sufficiently far away from the ends of the whole centrality range. For alternative curves for the  $R_{AA}^{J/\psi}$  with centrality we refer the reader to the review [23].

The different results in Figs. 7 and 8 take into account the charmonium suppression. It is clear from Fig. 8 that it is necessary and sufficient to include the charmonium suppression effects in order to describe the  $J/\psi$  peak correctly at all centralities. Since the  $R_{AA}$  ratios of the excited charmonium states are not yet measured, we have not implemented any correction for the  $\psi'$ .

Let us now turn our attention to the slope between the  $\phi$  and  $J/\psi$  peaks. From the discussion above it is clear that both the very low invariant mass ( $\pi^0$  Dalitz decay) as well as high invariant mass ( $J/\psi$ ) regions are fairly well described by the model. This is a good starting point to address the physics of the IMR in between.

In  $p + p$  collisions there is no medium that would distort the correlation among the emitted charm mesons and indeed, we have seen that the  $p + p$  data can be best described by assuming strong correlations among the  $D$  mesons. In central heavy-ion collisions on the other hand, there are several hundreds of hadrons emitted in each event and one would expect that the produced charmed hadrons interact with the surrounding medium thus destroying the initial correlations. We have studied the reinteractions of the charm mesons quantitatively within the HSD transport approach (cf. Ref. [23]) and have calculated the probability that neither of the two  $D$  mesons interacts with the surrounding medium. In this and only in this case the angular correlations among the emitted electrons and positrons would be preserved and remain similar to the  $p + p$  case.

Our results from the HSD calculations are shown in Fig. 11. The probability that the angular correlations remain the same as in  $p + p$  collisions is calculated as a function of collision centrality in  $Cu + Cu$  (open circles) and in  $Au + Au$  (filled circles) collisions at  $\sqrt{s_{NN}} = 200$  GeV. For practical purposes, we have parametrized these probabilities by the functions shown in the Figure. In the case of minimum bias  $Au + Au$  collisions, a proper weighted average over the whole centrality range (denoted by the filled square in Fig. 11) is used in our calculation instead of the explicit parametrization.

We can now study the invariant mass spectrum of the dilepton continuum in heavy-ion collisions in a more realistic scenario in which the slope of the IMR arises as a superposition of correlated and un-correlated open charm decays. All the three cases are shown for the minimum bias  $Au + Au$  collisions in the lower panel of Fig. 7. The result retaining the correlations like in  $p + p$  collisions is shown by the double dotted line in Fig. 7b, while the random

<sup>4</sup>  $R_{AA}^{AuAu} = 0.75 - 0.00137N_{Part}$   
 $R_{AA}^{CuCu} = 1.0 - 0.00516N_{Part}$

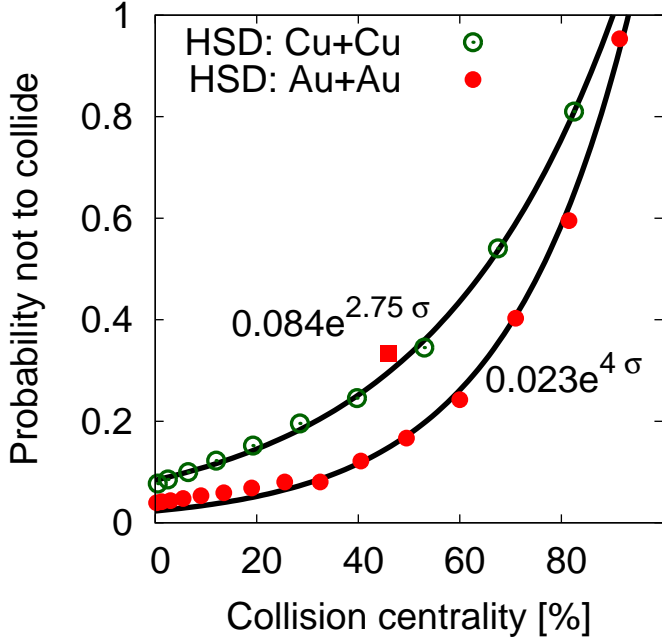


**Fig. 11.** (Color on-line) Probability that neither of the  $D$  and  $\bar{D}$  mesons collide with the surrounding medium in  $Cu + Cu$  (open circles) and  $Au + Au$  (closed circles) collisions at  $\sqrt{s_{NN}}=200$  GeV as evaluated with the HSD transport approach. The filled square denotes the value for minimum bias  $Au + Au$  collisions. The lines are parametrization that we have implemented in our calculations.

correlation case is represented by a dashed line. The solid line in between shows the invariant mass spectrum assuming that in 33% of the cases the dilepton pair stemming from the open charm decays retains the initial correlations while in 67% of the cases at least one of the  $D$  mesons has scattered and thus the correlation is destroyed. One can see that the most realistic case naturally interpolates between the two extreme cases and seems to describe the experimental data best (within the error bars).

Some further information on the IMR is gained by having an explicit look at the centrality dependence of the dilepton yield for  $Au + Au$  and  $Cu + Cu$  collisions at the top RHIC energy. The solid lines in Figure 13 are evaluated in this mixed scenario - based on the HSD rescattering calculations - and one can see that this approach practically underestimates the experimental spectra in the IMR for both systems.

Presently, we may only speculate that there seem to be further channels of possibly partonic nature in the IMR as suggested by several groups independently. Within thermal models this excess might be addressed as thermal dilepton radiation from the QGP [59] while also hadronic  $\rho + \rho$  or  $\pi + a_1$  scattering might contribute as suggested by van Hees and Rapp [7, 60]. The studies by one of the authors on explicit partonic reaction channels in Refs. [61, 62] allow for an implementation in the PHSD transport approach [63] which hopefully might clarify this issue in the near future.

In addition to the change in the angular correlations among the open charm mesons, also the magnitude of the (transverse) momentum of the  $D$  mesons can change due to interactions in the fireball. The PHENIX collaboration has measured the  $R_{AA}$  of single electrons coming from heavy quark decays [64] in  $Au + Au$  collisions and found that this  $R_{AA}$  is compatible with unity up to  $p_T$  of 2 GeV at all centralities. Thus, heavy-quark energy loss can (significantly) modify the di-electron yields in the IMR coming from  $D$  meson decays only at transverse momenta larger than 2 GeV.

In order to estimate how this affects our results, we have calculated the single electron + positron transverse momentum spectrum within the PHENIX acceptance and divided the results in four classes according to the corresponding invariant mass of the di-electron pair  $M_{e^+e^-}$ . The  $p_T$  spectra are shown in mass windows of  $M_{e^+e^-} \in [0,1]$ ;  $[1,2]$ ;  $[2,3]$  and  $[3,4]$  GeV in Figure 12. The solid lines indicate the results in the fully correlated case while the dashed lines are evaluated in the random correlation picture. All curves are normalized to unity. One can see that a significant fraction of electrons and positrons with  $p_T > 2$  GeV contributes to the invariant mass spectrum at invariant masses larger than 3 GeV, only. Our calculations concentrate on the region  $M_{e^+e^-} \in [0, M_{J/\psi}]$  and thus we can conclude that our results are only little affected by the heavy-quark energy-loss effects in the medium. In particular, the invariant mass region  $M_{e^+e^-} \in [1,2]$  GeV - in which our calculations under-estimate the measurements - appear little affected by the heavy-quark energy loss.

## 6 Discussion

As we have seen in the previous Section a scaling of the dielectron yields from  $p + p$  to heavy-ion collisions can lead to a surprisingly good description of the data in the peripheral collision systems but fails for the more central collisions. The question we wish to address here is that if we can, nevertheless, understand the observed excess in terms of hadronic degrees of freedom or if additional partonic production channels have to be incorporated.

According to the statistical hadronization model fits to  $p + p$  and  $Au + Au$  collisions at RHIC, the intensive thermal characteristics of these systems seem very similar at mid-rapidity. All of the light mesons decaying into dileptons are completely neutral and so the dilepton production rate does not actually depend on the chemical potentials at all and thus, besides the  $\gamma_S$  parameter discussed before, the temperature is the only intensive parameter left in the model that could lead to a non-trivial scaling behavior seen in the data. However, one of the lessons we have learned from the SHM fits to RHIC data is that the temperature is the same in heavy-ion collisions at all centralities and this temperature coincides with the one extracted from the  $p+p$  collision data. We have, nevertheless, checked that a moderate increase ( $T = 170 \rightarrow 190$  MeV) in temperature can not explain the observed excess in the LMR. One should notice that due to the momentum cut  $p_T > 0.2$  GeV the increase in temperature af-

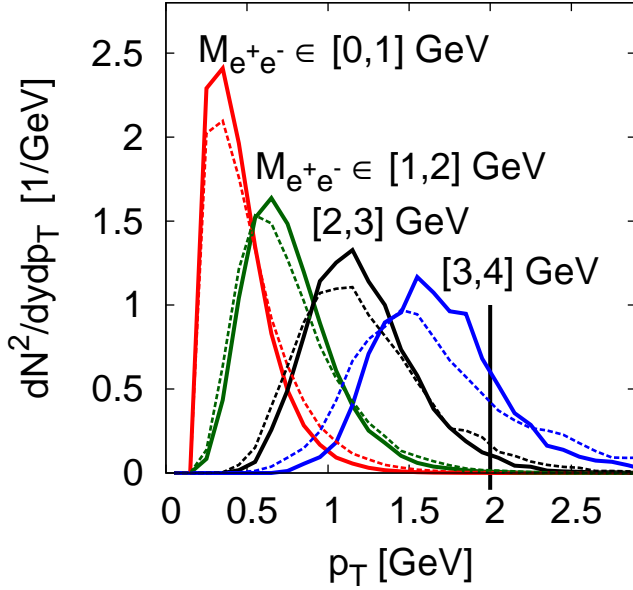


**Fig. 12.** (Color on-line) Transverse momentum distribution of electrons and positrons (within the PHENIX acceptance, normalized to unity) coming from semi-leptonic decays of  $D$  mesons in four different invariant mass windows  $M_{e^+e^-}$ . The solid lines indicate the spectra in the fully correlated case while the dashed lines arise in the random correlation picture. Electrons and positrons with  $p_T$  larger than 2 GeV (right from the solid vertical line) exhibit energy loss while propagating through the hot and dense medium [64].

fects more prominently the dilepton yields from the vector mesons than the emission from  $\pi^0$  and thus a change in temperature affects different regions in the invariant mass spectrum with different strength. One would nevertheless need unrealistically large temperatures of  $T > 200$  MeV if one attempts to assign the dilepton excess (seen by the PHENIX Collaboration) to an increase of the fireball temperature. We rule out such a possibility.

Independent previous model calculations [5, ?, 7] have been compared with the PHENIX data in the original publication [2] and we refer the reader to Figs. 41 and 42 of Ref. [2] for details. Our results agree qualitatively and also quantitatively with the previous model calculations in that the proton-proton collisions are well described in the whole invariant mass range while none of the analyses can explain the excess in the central heavy-ion collisions in the low invariant mass region. In extension of the previous studies we have, furthermore, investigated the possibility that the observed excess might stem from further semileptonic correlated kaon decays which are enhanced in central nucleus-nucleus collisions relative to proton-proton reactions by roughly a factor of three. Our upper limits for the dominant channels considered here clearly show that also these additional 'background sources' are not responsible for the large excess seen by the PHENIX Collaboration in central heavy-ion reactions.

The charmed sector or the IMR (if considered) has been treated essentially in a similar fashion by the PHENIX Collaboration as in this work and no solid conclusions have

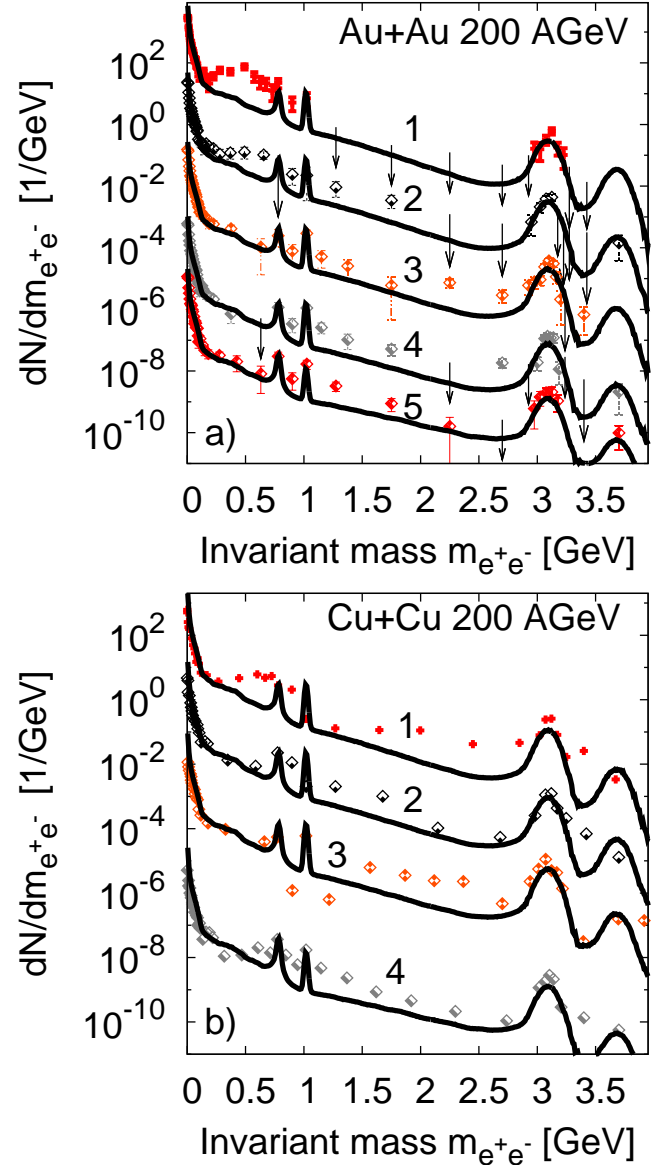


**Fig. 13.** (Color on-line) Invariant mass spectrum of pairs of electrons and positrons in  $Au + Au$  (top) [2] and  $Cu + Cu$  (bottom) [56] collisions at  $\sqrt{s_{NN}} = 200$  GeV in different centrality classes compared with model calculations. The centrality bins are labeled from central to peripheral as 1 (0-10%), 2 (10-20%), 3 (20-40%). Centrality bin 4 consist of (40-94%) and (40-60%) most central events in  $Cu + Cu$  and  $Au + Au$  collisions, respectively, while the centrality bin 5 includes (60-92%) most central collisions. Both the data and model calculational results are scaled with factors of  $10^4$  (0-10%),  $10^2$  (10-20%), 1 (20-40%),  $10^{-2}$  (40-60%) as well as  $10^{-3}$  (60-92%) and (40-94%) for clarity. The solid lines indicate the model results scaled from  $p + p$  collisions such that the charmed hadron yields are scaled with  $N_{bin}$  while the non-charmed hadron yields are scaled with  $N_{part}$  ( $Cu + Cu$ ) and with the fitted volume ( $Au + Au$ ) while correlations among the open charm hadrons are evaluated in the mixed procedure as described in the text. The starting point of the downward pointing arrows denote the data points which are defined as upper limits only.

been possible, so far. In order to go beyond the previous attempts we have calculated the rescattering probabilities of charm mesons dynamically (within HSD) which allows to estimate the amount of uncorrelated electron + positron pairs from  $D$  meson decays as a function of the centrality of the reaction. Our final results for  $Au + Au$  and  $Cu + Cu$  suggest that we clearly underestimate the preliminary yield from PHENIX which might point towards partonic sources - as suggested in Ref. [62] - in the intermediate mass regime.

So far we have considered only events with exactly one charmed quark pair. Processes leading to un-even amounts of charmed quarks are possible but they are more rare than the case we have studied and the corrections are probably not very large. Events with, e.g. 3  $D$  mesons tend to populate the low invariant mass region, in which the open charm contribution is insignificant, because in that case only one of the possible two "dilepton"-pairs is (strongly) correlated. To finally clear up the situation we are going to carry out non-perturbative calculations on correlated charm dynamics within the PHSD transport approach [63] that also includes the dynamics of charm quarks in the partonic phase.

## Acknowledgments

The authors like to thank A. Toia for stimulating discussions. Furthermore, E.L.B. and O.L. are grateful for financial support from the 'HIC for FAIR' center of the 'LOEWE' program and J.M. for support from DFG.

## References

1. A. Adare *et al.* [PHENIX Collaboration], Phys. Lett. B **670** (2009) 313.
2. A. Adare *et al.* [PHENIX Collaboration], Phys. Rev. C **81** (2010) 034911.
3. W. Ehehalt and W. Cassing, Nucl. Phys. A **602** (1996) 449.
4. W. Cassing and E. L. Bratkovskaya, Phys. Rept. **308** (1999) 65.
5. E. L. Bratkovskaya, W. Cassing and O. Linnyk, Phys. Lett. B **670** (2009) 428.
6. K. Dusling and I. Zahed, Phys. Rev. C **82** (2010) 054909.
7. H. van Hees and R. Rapp, Nucl. Phys. A **806** (2008) 339.
8. I. Kraus, J. Cleymans, H. Oeschler, K. Redlich and S. Wheaton, Phys. Rev. C **76** (2007) 064903.
9. F. Becattini, P. Castorina, J. Manninen and H. Satz, Eur. Phys. J. C **56** (2008) 493.
10. A. Andronic, F. Beutler, P. Braun-Munzinger, K. Redlich and J. Stachel, Phys. Lett. B **678** (2009) 350.
11. F. Becattini, J. Cleymans, A. Keränen, E. Suhonen and K. Redlich, Phys. Rev. C **64** (2001) 024901.
12. J. Cleymans, B. Kämpfer and S. Wheaton, Phys. Rev. C **65** (2002) 027901.
13. A. Baran, W. Broniowski and W. Florkowski, Acta Phys. Polon. B **35** (2004) 779.
14. J. Cleymans, B. Kämpfer, M. Kaneta, S. Wheaton and N. Xu, Phys. Rev. C **71** (2005) 054901.
15. J. Rafelski, J. Letessier and G. Torrieri, Phys. Rev. C **72** (2005) 024905.
16. A. Andronic, P. Braun-Munzinger and J. Stachel, Nucl. Phys. A **772** (2006) 167.
17. F. Becattini, J. Manninen and M. Gazdzicki, Phys. Rev. C **73** (2006) 044905.
18. J. Letessier and J. Rafelski, Eur. Phys. J. A **35** (2008) 221.
19. J. Manninen and F. Becattini, Phys. Rev. C **78** (2008) 054901.
20. A. Andronic, P. Braun-Munzinger and J. Stachel, Phys. Lett. B **673** (2009) 142 [Erratum-ibid. B **678** (2009) 516].
21. J. Noronha-Hostler, J. Noronha and C. Greiner, J. Phys. G **37** (2010) 094062.
22. G. Agakichiev *et al.* [CERES Collaboration], Eur. Phys. J. C **41** (2005) 475.
23. O. Linnyk, E. L. Bratkovskaya and W. Cassing, Int. J. Mod. Phys. E **17** (2008) 1367.
24. B. B. Back *et al.* [PHOBOS Collaboration], Phys. Rev. C **67** (2003) 021901.
25. J. Adams *et al.* [STAR Collaboration], Phys. Rev. Lett. **92** (2004) 112301.
26. I. G. Bearden *et al.* [BRAHMS Collaboration], Phys. Rev. Lett. **90** (2003) 102301.
27. F. Becattini, P. Castorina, A. Milov and H. Satz, Eur. Phys. J. C **66** (2010) 377.
28. C. Amsler *et al.* [Particle Data Group], Phys. Lett. B **667** (2008) 1.
29. I. G. Bearden *et al.* [BRAHMS Collaboration], Phys. Rev. Lett. **94** (2005) 162301.
30. S. S. Adler *et al.* [PHENIX Collaboration], Phys. Rev. C **74** (2006) 024904.
31. S. S. Adler *et al.* [PHENIX Collaboration], Phys. Rev. C **69** (2004) 034909.
32. G. Wolf, G. Batko, W. Cassing, U. Mosel, K. Niita and M. Schäfer, Nucl. Phys. A **517** (1990) 615.
33. K. Schmidt, E. Santini, S. Vogel, C. Sturm, M. Bleicher and H. Stocker, Phys. Rev. C **79** (2009) 064908.
34. E. L. Bratkovskaya and W. Cassing, Nucl. Phys. A **807** (2008) 214.
35. L. G. Landsberg, Phys. Rept. **128** (1985) 301.
36. R. K. Bhaduri, *Models of the Nucleon*, Addison-Wesley, Reading, MA (1988).
37. A. Spiridonov, arXiv:hep-ex/0510076.
38. J. Benecke, T.T. Chou, C.N. Yang and E. Yen, Phys. Rev. **188** (1969) 2159.
39. J. E. Elias, W. Busza, C. Halliwell, D. Luckey, P. Swartz, L. Votta and C. Young, Phys. Rev. D **22** (1980) 13.
40. G. J. Alner *et al.* [UA5 Collaboration], Z. Phys. C **33** (1986) 1.
41. B. B. Back *et al.*, Phys. Rev. Lett. **91** (2003) 052303.
42. A. M. Stasto, Acta Phys. Polon. B **38** (2007) 1031.
43. S. Alekhin, JETP Lett. **82** (2005) 628 [Pisma Zh. Eksp. Teor. Fiz. **82** (2005) 710].
44. S. J. Brodsky, J. F. Gunion and J. H. Kuhn, Phys. Rev. Lett. **39** (1977) 1120.
45. G. Torrieri, arXiv:0911.4775 [nucl-th].
46. A. Adare *et al.* [PHENIX Collaboration], Phys. Rev. Lett. **98** (2007) 232002.
47. A. Adare *et al.* [PHENIX Collaboration], Phys. Rev. D **82** (2010) 012001.
48. S. LaPointe [STAR Collaboration], Talk given in 26th Winter Workshop on Nuclear Dynamics.



49. J. Adams *et al.* [STAR Collaboration], Phys. Rev. Lett. **94** (2005) 062301.
50. A. Tai [STAR Collaboration], J. Phys. G **30** (2004) S809.
51. T. Sjostrand, S. Mrenna and P. Z. Skands, JHEP **0605** (2006) 026.
52. R. Seto [PHENIX Collaboration], J. Phys. G **30** (2004) S1017.
53. O. Linnyk, E. L. Bratkovskaya and W. Cassing, Nucl. Phys. A **830** (2009) 491c.
54. B. I. Abelev *et al.* [STAR Collaboration], Phys. Rev. C **80** (2009) 024905.
55. S. Afanasiev *et al.* [PHENIX Collaboration], arXiv:0706.3034 [nucl-ex].
56. S. Campbell [PHENIX Collaboration], Talk given in 26th Winter Workshop on Nuclear Dynamics.
57. A. Adare *et al.* [PHENIX Collaboration], Phys. Rev. Lett. **98** (2007) 232301.
58. A. Adare *et al.* [PHENIX Collaboration], Phys. Rev. Lett. **101** (2008) 122301.
59. E. V. Shuryak, Phys. Lett. B **78** (1978) 150 [Sov. J. Nucl. Phys. **28** (1978 YAFIA,28,796-808.1978) 408.1978 YAFIA,28,796].
60. H. van Hees and R. Rapp, Phys. Rev. Lett. **97** (2006) 102301.
61. O. Linnyk, J. Phys. G **38** (2011) 025105.
62. O. Linnyk, W. Cassing, E. L. Bratkovskaya and J. Manninen, arXiv:1012.0252 [nucl-th].
63. W. Cassing and E. L. Bratkovskaya, Nucl. Phys. A **831** (2009) 215.
64. A. Adare *et al.* [PHENIX Collaboration], arXiv:1005.1627 [nucl-ex].